Fabrication of novel Carbon Quantum Dots modified Bismuth Oxide (α-Bi_2O_3/C-dots): Material Properties and Catalytic Applications

Shelja Sharma[a], S. K. Mehta[a], A.O. Ibahdon[b], S. K. Kansal[c,*]

[a]Department of Chemistry and Centre of Advanced Studies, Panjab University, Chandigarh-160014, India

[b]Department of Chemical Engineering, University of Hull, Hull- HU6 7RX, United Kingdom

[c]Dr. S. S. Bhatnagar University Institute of Chemical Engineering and Technology, Panjab University, Chandigarh-160014, India

*Corresponding Author:

sushilkk1@yahoo.co.in; sushilkk1@pu.ac.in (S. K. Kansal)

Abstract

The present work reports the facile and the template free sonochemical synthesis of a novel catalyst, α-Bi_2O_3/C-dots, for the degradation of indigo carmine (IC) dye, its simulated dyebath effluent and levofloxacin under visible light catalysis. The compositional, structural, optical and morphological analysis of α-Bi_2O_3/C-dots was studied using analytical, spectroscopic and microscopic techniques. X-ray diffraction (XRD) results confirmed the presence of a monoclinic phase of α-Bi_2O_3 in the nanocomposite and crystallite size of 28.75 nm. Photoluminescence (PL) and UV-vis diffuse reflectance spectra (UV-DRS) studies showed good optical properties and a band gap of 2.49 eV. The synthesized photocatalyst showed superior visible-light driven photocatalytic activity for the degradation of indigo carmine dye (86% dye degradation in 120 minutes) compared to pure α-Bi_2O_3 (57%). α-Bi_2O_3/C-dots also exhibited 79% degradation of antibiotic drug levofloxacin within 120 minutes, under optimized conditions of pH, catalyst dose and initial dye concentration. Scavenger studies revealed that hydroxyl radicals and electrons played predominant roles in the photocatalytic degradation of IC dye. With respect to total organic carbon (TOC) analysis, 68.8% total organic carbon reduction of the IC dye (10 mg/L) was observed under the same experimental conditions. The catalytic efficiency of C-dots in the photocatalytic process is explained by proposing a degradation mechanism.

Keywords: α-Bi_2O_3/C-dots; Spectroscopy; X-ray diffractometry; Visible responsive, Photocatalysis; Indigo carmine; Dyebath effluent; Levofloxacin

1. Introduction

Semiconductor photocatalysis is regarded as a potential and green technology for mitigating environment pollution problems and eliminating residual water soluble contaminants by harnessing the entire solar spectrum [1]. Many wide-band gap semiconductors that can be stimulated under UV light only, such as ZnO, TiO_2, SnO_2 and WO_3 etc., have been studied extensively for the degradation of organic pollutants [2-4]. However, the major drawbacks associated with UV light active photocatalysts such as wide band gap, high recombination rate and inefficient charge separation, limit their applicability. Consequently, the exploration of visible light driven photocatalysts has become a necessity in order to meet promising industrial applications [5,6]. Many varieties of bismuth containing semiconductors have been exploited as efficient photocatalyst materials. For example, bismuth oxide (α-Bi_2O_3**)** has been used as a promising material for organic contaminants degradation owing to its low energy band gap, non-toxic nature, unique morphology, excellent optical properties and facile route of synthesis [7,8]. However, limited modifications have been carried out aimed at improving its photocatalytic performance. For example, nanostructures such as nanosheets and hollow mesoporous spheres can enhance the light-harvesting capability and provide more activity sites [9]. Moreover, other techniques such as ion doping and heterostructure assembly have proved to be beneficial in suppressing the charge carrier recombination in photocatalytic materials. In addition, up-conversion materials can also be considered to expand the optical spectrum response [10]. However, to the best of our knowledge and based on the information available in the literature, only a limited number of these techniques have been considered in practical applications in pollutant mitigations and novel nanostructures, fast charge separation and broad spectrum photocatalytic activity are highly needed in photocatalytic processes [11]. Consequently, recent

research has been focused on the use of hybrid nanostructured semiconductors, that are stable, non-toxic and efficient solar/visible light driven photocatalyst as these materials display efficient charge separation at the interface and expand the spectral response to a wide range of wavelengths [12-14].

In recent times, carbon quantum dots (C-dots) have been employed in photocatalysis due to their excellent photophysical and chemical properties such as wide absorption spectrum range, low toxicity, electron reservoir, photo-induced electron transfer properties and up-converted photoluminescence [15,16]. C-dots have the ability to enhance the photocatalytic activity of the conjugated parent photoctalyst to which it is attached to, by efficient charge separation, thereby suppressing the recombination of photogenerated charge carriers [17, 18]. C-dots act as good electron harvesters and converters, thus facilitating their energy band gap to a majority of photocatalysts [19]. A wide range of photocatalysts such as ZnO, TiO_2, Fe_2O_3, $BiFeO_3$, CuInZnS and BiOX (X= Cl, Br and I) have been known to show enhanced photocatalytic activity when attached to C-dots [20-25]. A number of bismuth based hybrid systems of C-dots have also been reported for photocatalytic degradation of organic pollutants. Di *et al.* demonstrated the synergistic effect of C-dots and Bi_2MoO_6 and reported the photocatalytic degradation of four different pollutants, ciprofloxacin, tetracycline hydrochloride, methylene blue and bisphenol A [26]. Tang *et al.* fabricated C-dots/m-$BiVO_4$ through hydrothermal and sonochemical technique and employed the nanocomposite for the removal of methylene blue dye [27]. Chen *et al*. synthesized C-dots/BiOI via hydrothermal approach and studied its photocatalytic activity for the degradation of methylene orange dye. Under optimized conditions, the experiments revealed that C-dots/BiOI showed 2.5 times higher photocatalytic efficiency than pure BiOI [28]. Zhao *et al.* modified BiOBr with C-dots and reported that BiOBr/C-dots showed 5.3 times higher photocatalytic efficiency

than pure BiOBr for the degradation of rhodamine B dye [29]. Additional work in this area is summarized in Table 1 to aid a clearer understanding of work carried out.

Table 1 Comparison of present work with literature.

Photocatalyst	Synthesis route	Surfactant /Substrate	Band gap	Photocatalytic activity	Reference
N-C-dots/$BiPO_4$	Ionic assisted solvothermal	[Omim]-H_2PO_4	4.11 eV (pure $BiPO_4$)	UV light irradiation, Ciprofloxacin degradation rate; 87.5% in 120 minutes	30
C-dots/Bi_2WO_6	Hydrothermal	CTAB	-	Photocatalytic reduction of CO_2 to CH_4 under NIR light	31
C-dots/ Bi_2WO_6	Electrochemical	PVP	-	Photocatalytic oxidation of acetone and toluene in 5 h under UV light irradiation	32
C-dots/$Bi_{20}TiO_{32}$	Solvothermal and oil bath reflux	Benzyl alcohol	-	Visible light irradiation, Isoproturon, Degradation rate; 98.1% in 60 h	33
C-dots/$BiVO_4$	Hydrothermal	-	2.7 eV	Photocatalytic generation of H_2 and O_2 under solar light irradiation	34
C-dots/BiOI	Sonochemical	[Bmim]I	-	Visible light irradiation, Degradation rate 76.8 % rhodamine B in 3 h, 99% bisphenol A in 2 h, 68% tetracycline in 2 h	35
C-dots/BiOCl	Immobilization	FTO	2.9 eV	Visible light irradiation, Rhodamine B, Degradation rate; 99% in 180 minutes	36
N-C-dots/ α-Bi_2O_3	Sol-gel	PS photonic crystal (template)	2.1 eV	Simulated sunlight irradiation, almost complete degradation of Rhodamine B	37
α-Bi_2O_3/C-dots	Sonochemical	-	2.49 eV	Visible light irradiation, Indigo carmine (IC) dye, Levofloxain; Degradation rate; 86% and 79% in 120 minutes	This work

In this study, we present a facile sonochemical synthesis of a novel photocatalyst (α-Bi_2O_3/C-dots), without the use of any surfactant/additive or chelating agent and characterized the prepared photocatalyst in detail using spectroscopic and analytical techniques. To the best of our knowledge,

this is the first study that reports the use of visible light responsive photocatalyst, i.e. α-Bi_2O_3/C-dots for the photocatalytic degradation of indigo carmine dye and levofloxacin (a fluoroquinolone drug).

2. Experimental section

2.1 Materials and methods

All the chemicals used were of analytical grade. The stock solutions of dye and drug were prepared in double distilled water. Levofloxacin was received from Saurav Chemicals, Derrabasi, India. The precursors, bismuth (III) nitrate pentahydrate ($Bi(NO_3)_3.5H_2O$, >99.0%) and L-Ascorbic acid ($C_6H_8O_6$, 99.0%) were procured from Sigma-Aldrich, India and Himedia, India, respectively. The model contaminant, IC dye (C.I. 73015), citric acid ($C_6H_8O_7$, 99.0%), sodium hydroxide (NaOH, 97.0%), sodium chloride (NaCl, 99.0%), sodium carbonate (Na_2CO_3, 99.0%), acetic acid (CH_3COOH, 99.0%), potassium dichromate ($K_2Cr_2O_7$, 99.0%) and isopropanol (IPA) (C_3H_8O, 99.0%) were procured from Merck, India.

2.2. Synthesis of α-Bi_2O_3 nanorods

Highly crystalline α-Bi_2O_3 nanorods were fabricated by facile and surfactant free sonochemical process. In the typical synthesis process, 5.0 g of bismuth nitrate pentahydrate was dispersed in 100 mL distilled water under continuous stirring. The precursor solution was magnetically stirred for half an hour to obtain a consistent white sol. The pH of obtained sol was about 2; it was changed to 10 by adding 5-M NaOH solution dropwise to the previous solution. Further the resultant solution was given ultrasonic treatment for an hour to ensure the uniform mixing. The color of white sol changed to yellow after ultrasonic stirring. Then the resultant mixture was kept for

stirring for overnight to obtain yellow precipitates. Since the reaction is pH dependent, the following reactions takes place:

$$Bi(NO_3)_3.5H_2O\ (s) \xrightarrow{pH > 9} Bi(OH)_3\ (s)$$

$$Bi(OH)_3\ (s) \longrightarrow Bi_2O_3\ (s) + H_2O$$

Then the resultant mixture was kept for stirring for overnight to obtain yellow precipitates. The precipitates were then collected by centrifugation and further washed with the mixture of distilled water and ethanol for several times and kept for drying in oven at 80^0C. Further, the yellow powder obtained was calcined at 450^0C for 2 hours.

2.3. Synthesis of C-dots

C-dots were synthesized by a hydrothermal process. L-ascorbic acid (0.25 g) and citric acid (0.25 g) were introduced into 50 mL of ethanol under magnetic stirring. 25 mL of water was added into the resultant reaction mixture and contents were then transferred into Teflon lined stainless autoclave and placed in oven at 160^0C for 3 hours. The solution obtained was kept at 4^0C for further use.

2.4 Synthesis of novel α-Bi_2O_3/C-dots nanocomposite

In the synthesis process of α-Bi_2O_3/C-dots, 50 µL C-dots (10 mg.mL^{-1}) were suspended in 100 mg of α-Bi_2O_3 and dispersed in 50 mL of ethanol. The reaction mixture was given ultrasonic treatment for an hour. Then the yellow product was collected, filtered off and several times with distilled water and ethanol and kept in oven for drying.

2.5 Characterization of catalyst materials

The general morphological analysis of the as-synthesized products was investigated by transmission electron microscopy (TEM; JEOL-JEM-2100F) and Field emission scanning electron microscopy (FESEM; HITACHI, SU8010 equipped with energy dispersive spectroscope (EDS) at an accelerating voltage of 10 kV. The crystalline characteristics and structural properties were investigated with X-ray diffraction (XRD; PANanalytical Xpert Pro.), assessed with Cu-Kα (λ= 1.54056 Å) at 45 kV and 40 mA by scanning at a rate of 2°(2θ) min^{-1}. The band gap of the photocatalysts was computed from Shimadzu UV-2600 ultraviolet–visible diffuse reflectance (DRS) spectra using barium sulfate as a standard material. Functional groups and surface composition were analyzed by Fourier transform infrared (FTIR) spectroscopy with Thermoscientific (Nicolet iS50), equipped with a diamond ATR in the wavenumber ranging from 400–4000 cm^{-1}. Thermogravimetric analysis was carried out using TGA/DSC analyzer, Perkin-Elmer STA 6000 in the temperature range of 0 to 1000 °C at an acceleration speed of 10 °C min^{-1}. Photoluminescence (PL) spectrum was recorded on Hitachi F-7000; 5J1-004 model with quartz cuvette of 1 cm path length. The mineralization of dye was calculated by determining total organic carbon (TOC) from TOC-L CPN Shimadzu analyzer. The UV–vis absorption spectra were recorded on Systronics 2202 spectrophotometer using quartz cuvette of volume 4 mL.

2.6 Photocatalytic experiments

The photocatalytic properties of α-Bi_2O_3/C-dots was examined by studying the degradation of an acidic IC dye and levofloxacin under visible light illumination with 85 W Oreva CFL bulb lamp inclusive of UV cut-off filter with intensity 4150 lumens and wavelength ranging from λ=450–650 nm. α-Bi_2O_3/C-dots concentrations varying from 0.5 g/L-1.25 g/L, was dispersed in 100 mL of IC dye/levofloxacin (10 mg/L) and placed in the dark for 30 minutes in order to achieve adsorption- desorption equilibrium under magnetic stirring. Photocatalytic degradation

commenced by irradiating the solution with visible lamp and samples of the solution were withdrawn at specific time intervals with a syringe and filtered through 0.45 µM Chromafil filter. The concentration of the solution was determined using Systronics-2202 UV-vis spectrophotometer. The operational parameters such as pH of pollutant solution, initial concentration of contaminant and dose of catalyst were optimized. All photocatalytic experiments were performed in duplicate for precision and accuracy.

The rate of degradation (%) was calculated from the equation below:

$$\text{Degradation rate (\%)} = \frac{C_o - C_t}{C_o} \boldsymbol{X\ 100}$$

Where C_0 is the concentration of pollutant before visible light illumination and C_t is the concentration of pollutant at a specific time t of visible light irradiation.

Furthermore, the function and occurrence of radical reactive species was determined using various scavengers ($K_2Cr_2O_7$, NaCl and IPA). 0.01 M of scavengers were added to the dye solution, prior to illumination and addition of catalyst.

3. Results and discussion

3.1 Crystal structure of the as-synthesized photocatalysts

The structural and crystal properties of the synthesized samples were investigated by XRD analysis. The XRD pattern of synthesized C-dots is shown in Fig. 1a. A broad diffraction peak located at $2\theta = 20^0$ with spacing of 0.34 nm was observed, indicating 002 planes of graphitic structure and amorphous nature of C-dots [38]. Fig. 1b represents the XRD pattern of the synthesized α-Bi_2O_3/C-dots nanocomposite. It was observed that α-Bi_2O_3 possessed a monoclinic structure along with space group of P21/c. All the diffraction peaks in the XRD pattern located at

2θ = 21.8, 24.6, 25.8, 26.9, 27.3, 28, 32.5, 33, 35, 45.1, 46.3, 52.3 and 54.79 were indexed to (002), (-102), (002), (111), (120), (012), (-211), (-122), (-212), (023), (041), (-322) and (-241) lattice planes, respectively. The obtained peaks were found to be in agreement with literature and JCPDS No. 71-2274 [39]. Apart from the peaks attributable to monoclinic α-Bi_2O_3, there were no other diffraction reflections observed, suggesting that the synthesized catalyst was of high purity. Also, the introduction of C-dots did not result in any change or shift in the structure of α -Bi_2O_3which suggested low concentrations of C-dots in α-Bi_2O_3. The crystallite size (D) of the α-Bi_2O_3/C-dots was computed from the Debye-Scherrer's equation and found to be ~28.75 nm. The interplanar spacing (d_{hkl}); (h, k and l are the Miller indices of adjacent plane) of the atomic lattice and can be computed from Bragg's Law as follows:

$2\ d_{hkl} = n\ \lambda \sin\theta$; n is an integer.

For monoclinic structure, following crystal geometry equation was applied to determine the lattice constants "a", "b" and "c".

$$1/(d_{hkl})^2 = h^2/a^2 \sin^2\beta + k^2/b^2 + l^2/c^2 \sin^2\beta - 2hl \cos\beta/ac \sin^2\beta$$

The values of lattice constants, i.e. "a", "b" and "c" were computed as 5.8485 Å, 8.1556 Å and 7.5225 Å, respectively.

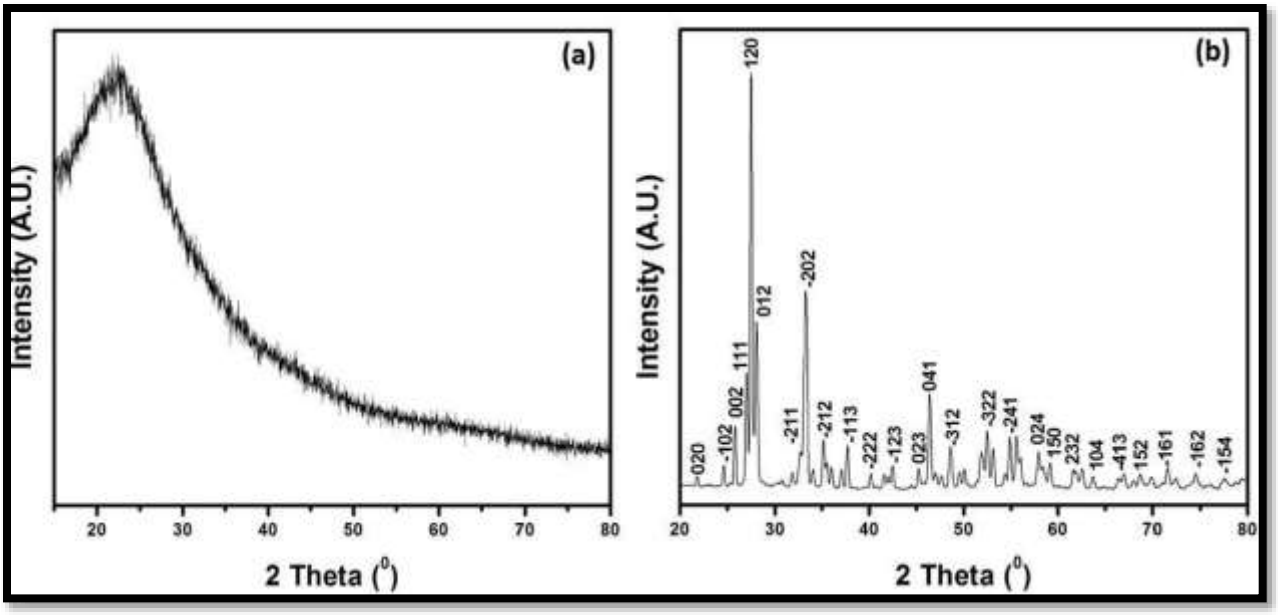

Fig. 1 Typical XRD pattern of (a) C-dots and (b) α-Bi_2O_3/C-dots

3.2 Morphological analysis of α-Bi_2O_3/C-dots

The structural characteristics and general morphologies of α-Bi_2O_3, C-dots and α-Bi_2O_3/C-dots was studied by FESEM and TEM microscopy. The results obtained are shown in Fig. 2. FESEM images of pure α-Bi_2O_3 are shown in the supporting information (Fig. S1). As can be seen in Fig. 2a and b, α-Bi_2O_3 possessed rod like morphology over which nanoparticles of C-dots were assembled. It can also be shown that α-Bi_2O_3/C-dots exhibited high aspect ratio. The surfaces of rods are not as smooth compared to pure α-Bi_2O_3 due to the dense agglomeration of nanoparticles of C-dots over the surface. The typical length of rods was estimated to be 9-10 μm and diameters were found to be in the range of 100 nm approximately. In Fig. 2c and d, in the high resolution images, accumulation of nanoparticles of C-dots over the rods could be seen, indicating the uniform growth of C-dots over α-Bi_2O_3 nanorods. The TEM images of α-Bi_2O_3/C-dots are in good agreement with FESEM results with respect to morphologies and dimensions. Results show that

C-dots are monodispersed with particle sizes less than 10 nm, as indicated by the TEM image of pure C-dots (Fig. S1). Growth of nanoparticles of C-dots over the surface of α-Bi_2O_3 nanorods can be observed. In addition, since the nanorods of α-Bi_2O_3 possess high density, agglomeration of a cluster of nanoparticles over the surfaces of nanorods can be barely seen in the high resolution TEM image of α-Bi_2O_3/C-dots (Fig. 2f).

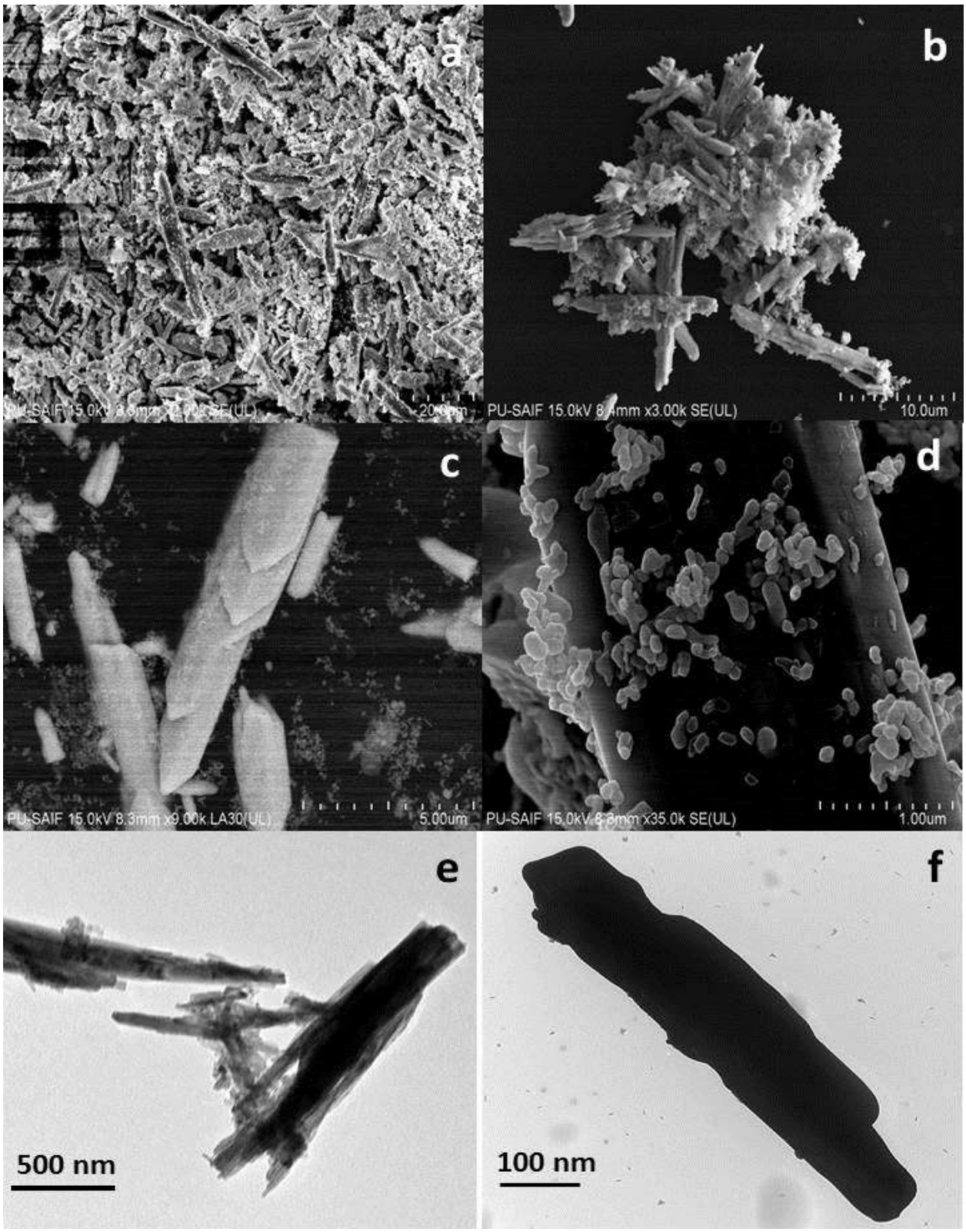

Fig. 2. FESEM image of α-Bi_2O_3/C-dots (a,b) at low magnification representing high growth (c,d)

at high magnification. TEM micrographs of α-Bi_2O_3/C-dots (e) at low and (f) high magnification

3.2 Elemental and compositional analysis of α-Bi_2O_3/C-dots

The elemental composition of the sample prepared (α-Bi_2O_3/C-dots) was confirmed by energy dispersive spectroscopy (EDS) analysis. EDS pattern of α-Bi_2O_3/C-dots indicated the presence of bismuth, oxygen and carbon in the sample, without any impurity (Supporting Information, Fig. S2). The selected area elemental mapping of α-Bi_2O_3/C-dots was also carried out. It can be observed in Fig. 3 that the sample consists of three distributed elements (Bi, C and O) in different ratios and amounts and have dense and direct contact with each other.

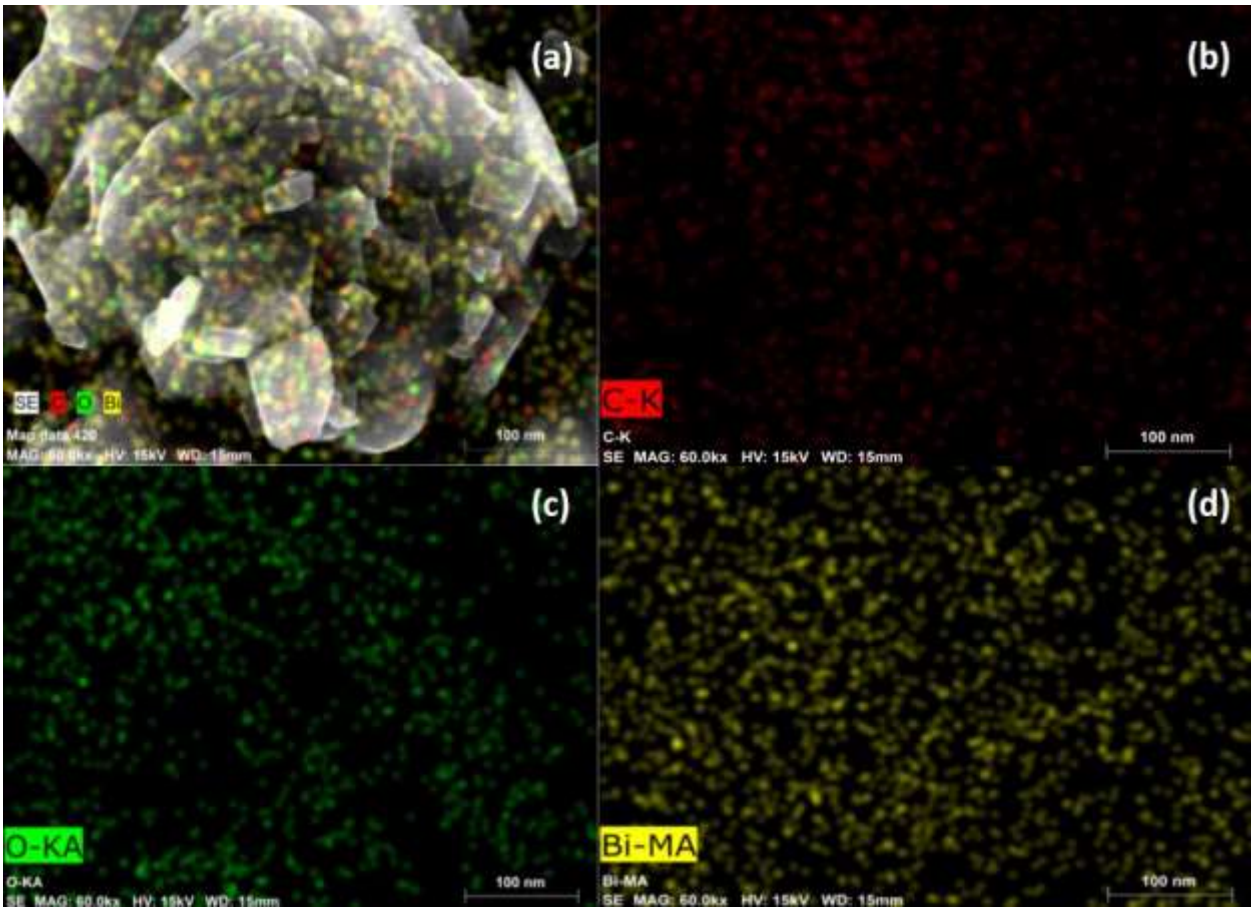

Fig. 3 Elemental mapping of α-Bi_2O_3/C-dots.

The chemical composition of the prepared photocatalysts and interactions between α-Bi_2O_3 and C–dots were analyzed by FTIR. Fig. 4a depicts the FTIR spectra of α-Bi_2O_3 and α-Bi_2O_3/C-dots. In the FTIR spectrum of α-Bi_2O_3, many well defined peaks were observed. The sharp and intense peak at 1380 cm^{-1} could be ascribed to the C=O vibrations of the precursor [40]. The peaks at 846 cm^{-1} and 414 cm^{-1} were ascribed to the vibrations of Bi-O bonds of α-Bi_2O_3 [39,40]. Additional characteristic peaks were observed in the FTIR spectrum of α-Bi_2O_3 /C-dots. The peaks at 2197 cm^{-1} and 1601 cm^{-1} are associated with the stretching vibrations of the C-H group and vibrating mode of hydroxyl groups, -OH, implying the existence of C-dots [41]. Moreover, the peak at 845 cm^{-1} was found to be diminishing in case of α-Bi_2O_3 /C-dots, due to the interactions between Bi-O bond of α-Bi_2O_3 and C-O surrounding of C-dots. This is attributed to the difference in the concentrations of nanocomposite (α-Bi_2O_3/C-dots) and pure α-Bi_2O_3, indicating that the position of the FTIR peaks remained intact, although the magnitude of intensity got decreased.

3.3 Thermal and optical properties of α-Bi_2O_3*/C-dots*

In order to examine the thermal stability of α-Bi_2O_3/C-dots, TGA was carried out (Fig. 4b). The TGA curve showed two weight loss regions. The total weight loss up to 1000^0C is approximately 24%. Two minor weight losses of 4.225% and 3.143 % up to 800^0C are ascribed to the desorption of H_2O molecules bound to the surface of the photocatalyst [42]. An additional significant weight loss between 800^0C and 1000^0C, of 16.94% was likely due to the decomposition of oxygen containing functional groups [43].

The photophysical properties of the synthesized catalysts, α-Bi_2O_3 and α-Bi_2O_3/C-dots, was investigated by recording room temperature PL spectra at λ_{ex}= 300 nm as shown in Fig. 4c. For α-Bi_2O_3, three emission peaks in the visible region were observed, a sharp emission band at 470 nm

and two broad shoulder bands at 424 nm and 530 nm. The broad band at 424 nm was ascribed to the recombination of photoinduced charge carriers [44]. The distinctive peaks at 470 nm and 530 nm were due to the presence of oxygen vacancies owing to the crystal defects over surface [45]. In the case of α-Bi_2O_3/C-dots, there was a disappearance of emission band at 424 nm, which implied that α-Bi_2O_3/C-dots can efficiently lower the chances of direct recombination of photogenerated charge carriers, thereby improving the photocatalytic activity of α-Bi_2O_3/C-dots.

The light absorption studies of synthesized catalysts can be explained on the basis of UV-vis DRS studies. Fig. S3 shows the UV-DRS spectra of α-Bi_2O_3 and α-Bi_2O_3/C-dots in the wavelength ranging from 200-800 nm. It can be observed that the spectrum of α-Bi_2O_3 exhibited a significant absorption edge with wavelength shorter than α-Bi_2O_3/C-dots, which might be attributed to the intrinsic band gap absorption. However, in the case of the α-Bi_2O_3/C-dots, the absorption was found to shift more towards the visible region and their absorption intensity was also greater than α-Bi_2O_3. This might be due to the fact that the carbon atoms were found to occupy the interstitial sites of the α-Bi_2O_3 lattice, which could lower the value of the band gap [46]. Also, Using Kubelka-Munk function, $(\alpha h\upsilon)^2$ was plotted against $h\upsilon$. As shown in Fig. 4d, it was observed that α-Bi_2O_3 showed 2.7 eV band gap, whereas α-Bi_2O_3/C-dots exhibited a band gap of 2.49 eV. The lower value of the band gap for α-Bi_2O_3/C-dots compared to α-Bi_2O_3 indicates the higher absorption capacity of α-Bi_2O_3/C-dots [37]. Hence, from the results obtained results it can be inferred that α-Bi_2O_3/C-dots can be used in visible light catalyzed reactions. The experimental results obtained are in agreement with literature and further provided evidence for the successful formation of α-Bi_2O_3/C-dots [25].

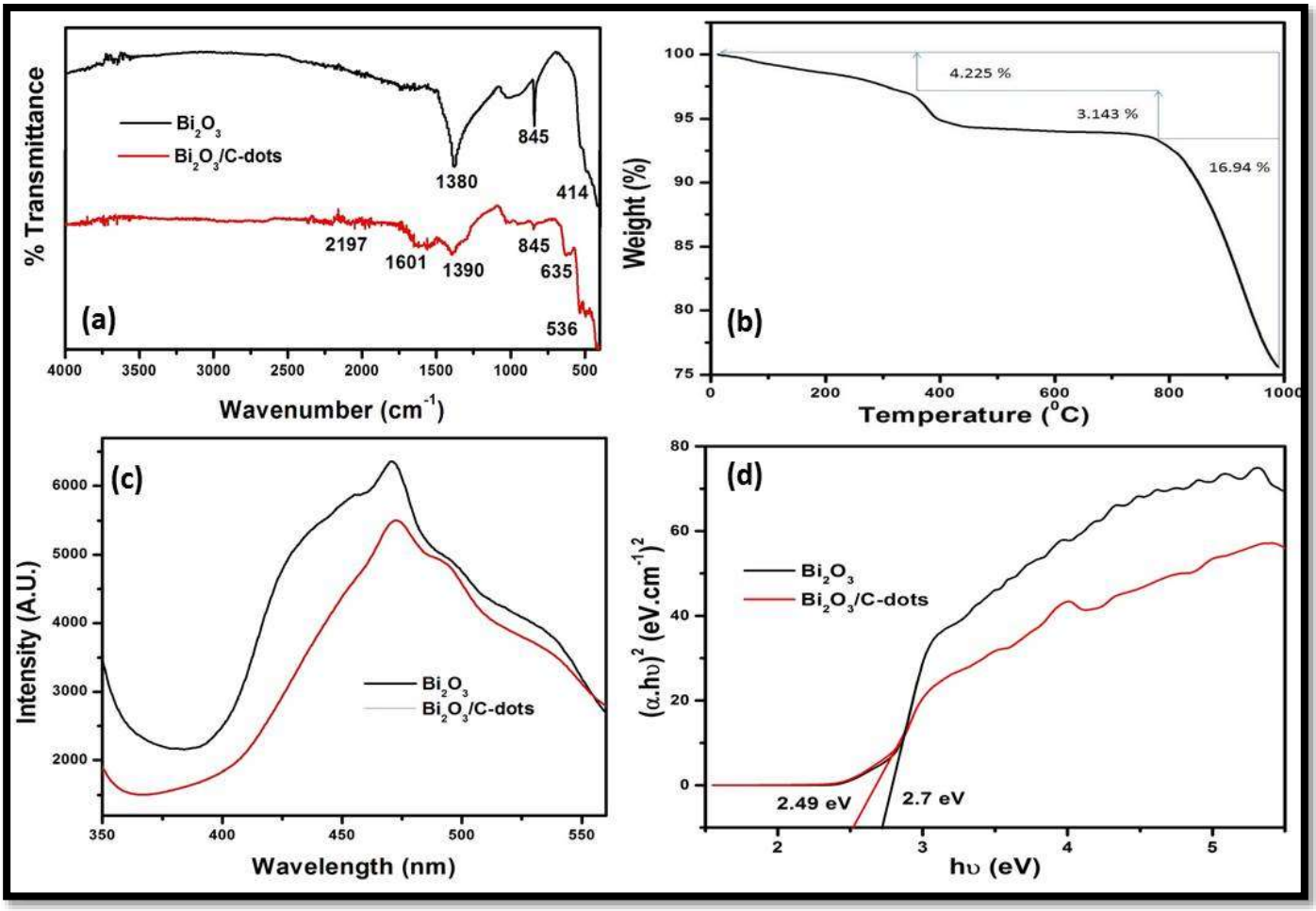

Fig. 4. (a) Typical FTIR spectra of α-$Bi_2O_3$and α-Bi_2O_3/C-dots (b) TGA curve of α-Bi_2O_3/C-dots (c) PL spectra of α-$Bi_2O_3$and α-Bi_2O_3/C-dots (λ_{ex}= 300 nm) (d) Kubelka-Munk transformed reflectance spectra α-$Bi_2O_3$and α-Bi_2O_3/C-dots

3.5 Evaluation of the photocatalytic activity of α-Bi_2O_3 and α-Bi_2O_3/C-dots

To investigate the photocatalytic activity of the photocatalysts, IC dye was chosen as model contaminant. IC, an indigoid dye, is widely used as a colouring agent and an additive in pharmaceuticals, textile and food industries. Inhalation of IC is harmful as it is carcinogenic and can cause severe health problems such as hypertension, cardiovascular disease and gastrointestinal tract infections [47]. IC dye shows maximum absorbance at wavelength 612 nm. Fig. 5a shows the

UV-vis absorbance spectra of the dye at different time intervals using α-Bi_2O_3/C-dots as a photocatalyst. The absorbance at λ_{max} was found to diminish during the course of the reaction and results show that 86% of the dye was degraded in 120 minutes under visible light illumination. Control experiments in the dark and without catalyst were also performed to investigate the effect of light source and catalyst in the photocatalytic process. It was observed that almost no degradation occurred in the absence of α-Bi_2O_3/C-dots under visible light only (Fig. 5b). This shows that photolysis was inefficient for the degradation of the dye, with only about 10% of dye degradation in 120 minutes. In addition, the photocatalytic degradation of IC dye was performed with pure α-Bi_2O_3 without C-dots. Results show that 57% of the dye was decomposed in 120 minutes under visible light illumination, whereas α-Bi_2O_3/C-dots showed 86% degradation under the same experimental conditions (Fig. 5b). Hence, α-Bi_2O_3/C-dots under visible light illumination have shown to be highly efficient for the photocatalytic degradation of IC dye and this is enhanced by the presence of C-dots in the nanocomposite.

Process parameters including catalyst dose, initial concentration of pollutant and pH of the dye and drug solution were also optimized as the parameters have an impact on the photocatalytic efficacy of the catalyst. To determine the optimum quantity of catalyst for visible light responsive photocatalytic decomposition of IC dye, the amount of α-Bi_2O_3/C-dots was changed from 0.5 g/L to 1.25 g/L at the natural pH (6) and dye concentration (10 ppm) (Fig. 5c). It was deduced that with the change in the dose of catalyst from 0.5 to 1 g/L, the degradation rate of IC dye also increased from 57% to 86%, due to the increased accessibility of active sites on the surface of photocatalyst for photodegradation reaction. However, with a further increase in dose of photocatalyst to 1.25 g/L, the degradation declined to 83%. This might be due to the undesired

scattering of light caused by increased turbidity in dye solution which hindered the pathway of photons to reach the surface of substrate, indicating the optimum dose of catalyst to be 1 g/L.

The photocatalytic degradation of IC dye was also examined by varying the pH of aqueous solutions of dye while other parameters were held constant (Fig. 5d). Results show that 86% of the dye was degraded at natural pH. However, at a pH of 4, the photocatalytic degradation was 82.5% and at a pH of 9, the photocatalytic degradation decreased from 86% to 80.8%, suggesting an optimal pH of 6 for photocatalytic testing.

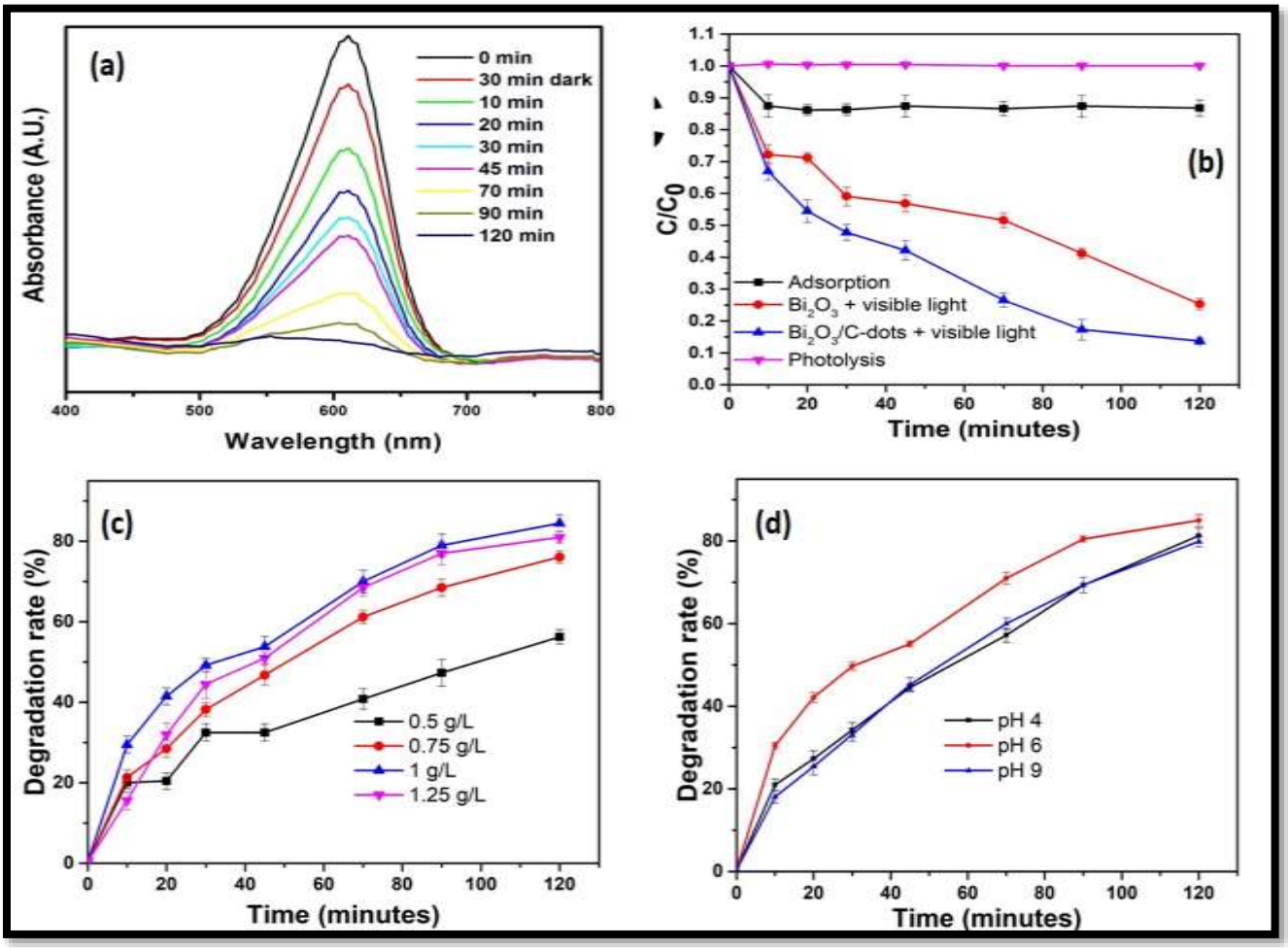

Fig. 5. (a) Time dependent UV-vis absorbance spectra of IC dye (10 mg/L, pH 6, 1 g/L α-Bi_2O_3/C-dots dose) (b) Photolysis, adsorption and photocatalysis affecting degradation rate of IC dye (c) Effect of catalyst dose and (d) pH on the degradation rate (%) of IC dye

The influence of the variation in initial dye concentration on the photocatalytic performance of α-Bi_2O_3/C-dots was examined at an optimized natural pH (6) and catalyst dose (1 g/L) (Fig. 6a). It was observed that as the concentration of dye increased from 10 ppm to 20 ppm, the degradation decreased from 86% to 80% and with an additional increase in dye concentration from 20 ppm to 30 ppm, the degradation decreased to 77%. This is attributed to the increased concentration of dye under constant catalyst dose, light source and intensity, resulting in reduced penetration of photons. Also, the rate of degradation decreased due to the adsorption of dye molecules on the surface of α-Bi_2O_3/C-dots, leaving a reduced catalyst surface for photon penetration.

Furthermore, cyclic photocatalytic experiments were also performed to determine the reusability and stability of the catalyst, i.e. α-Bi_2O_3/C-dots (Fig. 6b). For this purpose, the catalyst was collected from the reaction medium and thoroughly washed many times with distilled water, filtered and desiccated at 80^0C for drying. The photocatalytic degradation of the dye over three consecutive cycles was 86%, 83.25% and 81%, respectively. A slight fall in the photocatalytic activity of α-Bi_2O_3/C-dots was observed after each cycle, suggesting that the prepared catalyst exhibited high photocatalytic efficiency in the degradation of the IC dye

In addition to the degradation experiments, scavenger radical studies were executed to ascertain the nature of the active radical species which might be responsible for the photocatalytic decomposition of IC dye (Fig. 6c). Different scavengers including $K_2Cr_2O_7$ (scavenger for

electrons; e^-), NaCl (scavenger for holes; h^+) and IPA (scavenger of hydroxyl radicals; ·OH) were investigated for this purpose. The photocatalytic degradation of the dye without any scavenger was 86% and this decreased to 58%, 59% and 80% in the presence of IPA, $K_2Cr_2O_7$ and NaCl, respectively. The results obtained demonstrate that ·OH and e^- are dominating and are the primary reactive species in the photocatalytic decomposition of IC dye.

The photocatalytic degradation was also studied using the Langmuir- Hinshelwood kinetic model,

$$\ln (C_0/C_t) = kt$$

where C_0 is the initial concentration and C_t is the final concentration of IC dye at time (t) and *k* is the reaction rate constant. The photocatalytic degradation of IC dye conforms to a pseudo first order kinetics and the rate constant *k* calculated from the slope was 0.01734 min^{-1} (Fig. 6d).

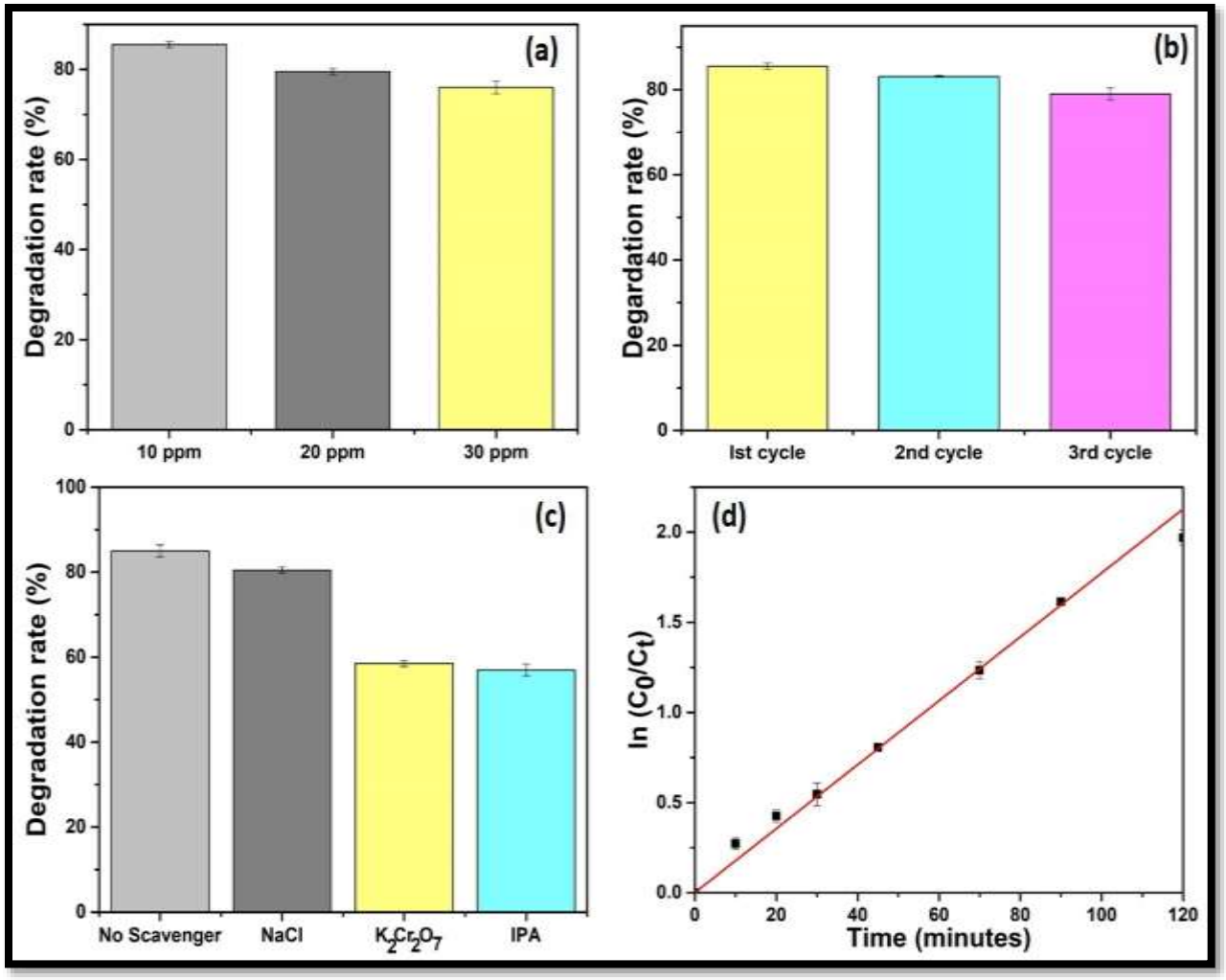

Fig. 6. (a) Effect of initial dye concentration on the photocatalytic degradation rate of IC dye in presence of α-Bi_2O_3/C-dots (pH 6, catalyst dose 1 g/L) (b) Recyclability of α-Bi_2O_3/C-dots for the degradation of IC dye up to three consecutive cycles. (c) Effect of different scavengers on the degradation rate if IC dye using α-Bi_2O_3/C-dots (10 mg/L IC dye, natural pH, 1 g/L catalyst dose). (d) Reaction kinetic studies for the photocatalytic degradation of IC dye.

The mineralization of the dye was determined by total organic carbon (TOC) analysis. The estimated initial TOC value of the dye solution (10 mg/L) was 7.245 mg/L and after 120 minutes, the TOC decreased to 2.256 mg/L. It can be estimated that approximately 68.8% TOC reduction

of dye solution was observed within 120 minutes of visible light in the presence of α-Bi_2O_3/C-dots (1 g/L) and hence, the results confirmed the mineralization of IC dye. The TOC measurement would therefore appear to be an appropriate technique for assessing the detoxification of contaminated water.

In order to correlate the present study with the real life situations in textile and pharmaceutical processing, a simulated dyebath effluent solution was prepared. The chemical composition of the dyebath effluent solution is shown in Table S1 in the supporting information. The photocatalytic activity of α-Bi_2O_3/C-dots towards the dyebath solution was determined using a dyebath of concentration of 10 ppm and a catalyst dose of 1 g/L. Approximately 87% of the dye was degraded within 180 minutes of visible light irradiation using α-Bi_2O_3/C-dots. Fig. 7a shows the UV-vis absorbance spectra of the dyebath effluent at different time intervals. From the results obtained, it can be concluded that α-Bi_2O_3/C-dots exhibited enough photocatalytic potential for the treatment of industrial wastewater. The kinetics of the photocatalytic degradation of the dyebath effluent was also studied (Supporting Information, Fig. S4). It was observed that the degradation followed pseudo first order kinetics, with a rate constant (k) of 0.0120 min^{-1} and an R^2 value of 0.9940.

The photocatalytic efficiency of α-Bi_2O_3/C-dots towards levofloxacin (a fluoroquinolone antibiotic drug) was also evaluated under visible light irradiation. It can be interpreted from the spectra that the absorbance of levofloxacin gradually decreased with irradiation time (Fig. 7b). Approximately 79% (10 mg/L (conc. of drug), pH 7, catalyst dose 1g/L) levofloxacin was degraded within 120 minutes of visible light irradiation with combination of phenomena of adsorption and photocatalysis.

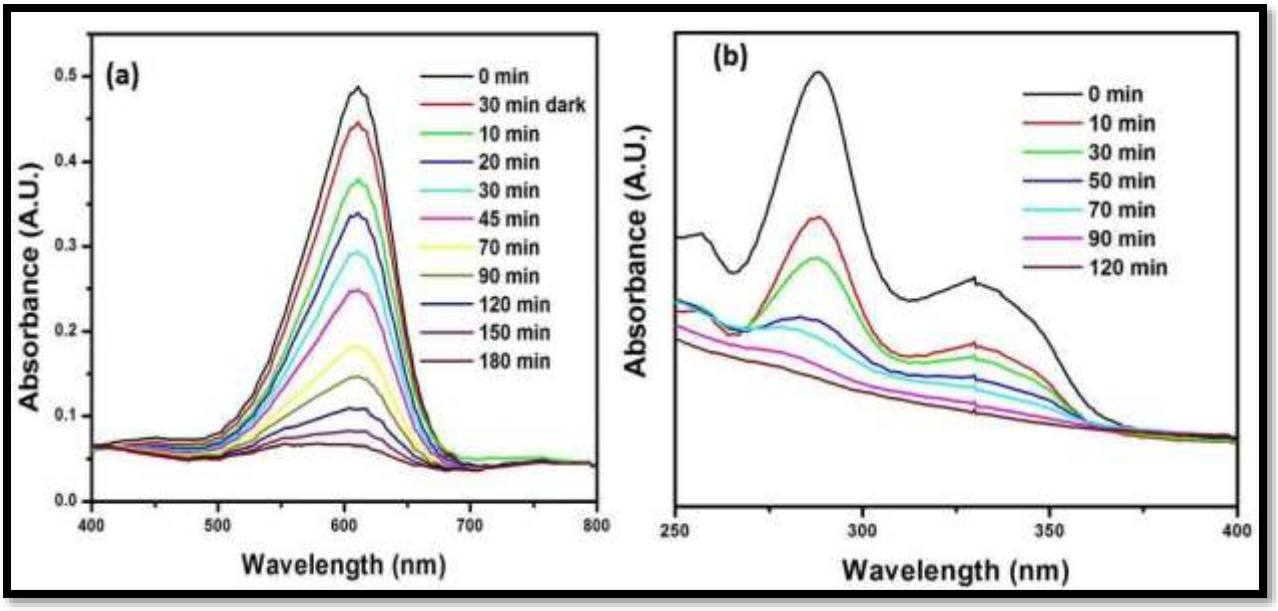

Fig. 7. Time dependent UV-vis absorbance spectra of (a) simulated dyebath effluent of IC dye (IC dye 10 mg/L, neutral pH) under visible light irradiation in the presence of α-Bi_2O_3/C-dots (catalyst dose 1 g/L). (b) levofloxacin (10 mg/L, 7 pH) in presence of α-Bi_2O_3/C-dots (catalyst dose 1 g/L).

3.6 Proposed pathway for the photocatalytic performance of α-Bi_2O_3/C-dots

The improved photocatalytic performance of α-Bi_2O_3/C-dots demonstrated the importance of C-dots in the photocatalytic process and it can be inferred that α-Bi_2O_3/C-dots exhibited strong visible light absorption capacity because of the C-dots in the nanocomposite. The up-conversion property and superior visible light response of C-dots have enabled the conversion of longer to shorter wavelength excitation meaning that α-Bi_2O_3 was able to generate electrons and holes. Due to the photoinduced electron migration characteristic of C-dots, it can serve as electron donors as well as acceptors, which can competitively prevent the recombination of photogenerated electrons and holes and enhance the photocatalytic activity of the nanocomposite. These observations are also

supported by PL, UV-vis and DRS results. The good separation efficiency increase the lifetime of the photogenerated charge carriers by obstructing the recombination of electrons and holes, leaving enough charge carriers to produce highly reactive species and substantially enhance the photocatalytic activity of α-Bi_2O_3/C-dots [17,20]. Upon illumination, the electrons excited from the valence band to the conduction band of α-Bi_2O_3 are transferred to the C-dots leaving holes in the valence band and thereby preventing the recombination of electrons and holes. The band edge positions of α-Bi_2O_3/C-dots were calculated by the empirical formula written below:

$$E_{VB} = X_e - E_e + 0.5\, E_g$$

$$E_{CB} = E_{VB} - E_g$$

where E_{VB} and E_{CB} are the valence band and conduction band edge potentials of α-Bi_2O_3/C-dots, E_e (4.5 eV) is the energy of free electrons on hydrogen scale, X_e is the electronegativity and E_g (2.49 eV) is the calculated band gap of α-Bi_2O_3/C-dots. The corresponding band edge potentials, E_{VB} and E_{CB} were estimated to be 2.695 eV and 0.205 eV, respectively. Since, the E_{VB} of α-Bi_2O_3/C-dots (2.695 eV) is more positive than the standard redox potential of $\cdot OH/OH^-$, (1.99 eV vs NHE), this implies a higher oxidizing capability.

The photogenerated electrons on the surface of C-dots reacted with adsorbed oxygen and formed superoxide radical anions, which upon protonation, produced highly reactive hydroxyl radicals. Photogenerated holes also generated hydroxyl radicals by reacting with adsorbed water molecules. These highly oxidizing reactive species are capable of degrading organic pollutants efficiently as illustrated schematically in Fig. 8.

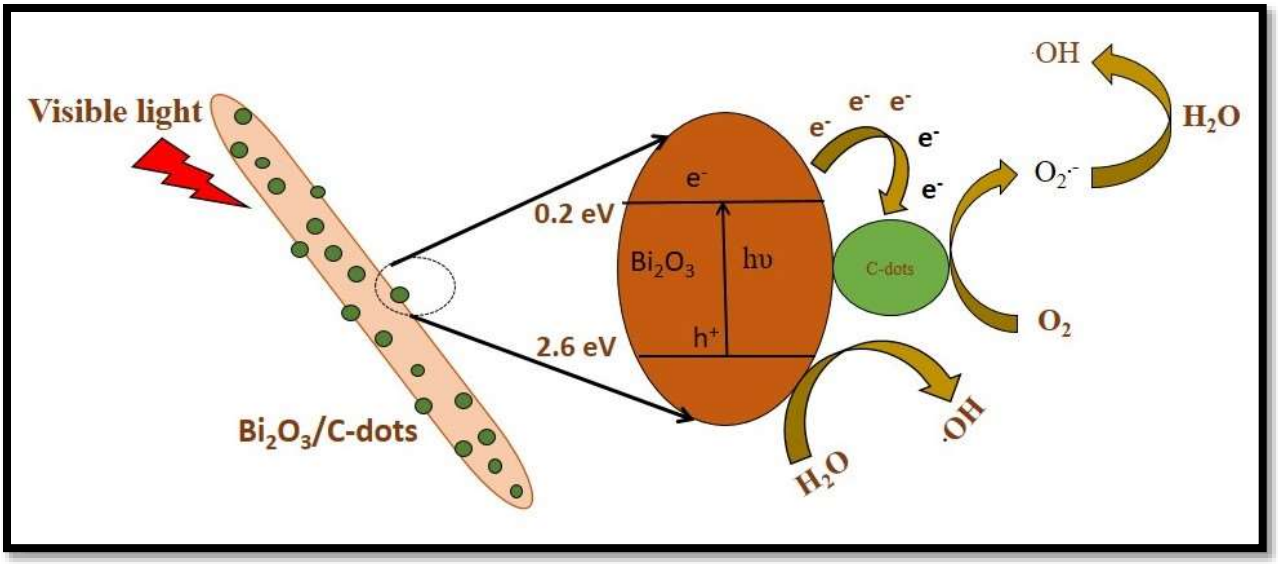

Fig. 8. Proposed photocatalytic mechanism of α-Bi_2O_3/C-dots under visible light

4. Conclusions

The synthesis of new or novel catalyst materials for use in environmental remediation of toxic pollutants is of high importance, especially in the processing industry. Consequently, on the basis of reported synthetic protocols for photocatalyst materials, we have chosen a surfactant free sonochemical method to synthesize a novel α-Bi_2O_3/C-dots. XRD analysis of this novel catalyst material showed high crystallinity and purity, FTIR studies confirmed the successful modification of α-Bi_2O_3 with C-dots, PL and TGA analysis showed excellent optical and thermal properties of the photocatalyst. Nanorod shaped α-Bi_2O_3/C-dots exhibited a band gap of 2.49 eV, implying that the catalyst can be used for visible light catalyzed reactions for the treatment of pharmaceutical wastewaters. It was observed that α-Bi_2O_3/C-dots exhibited enhanced photocatalytic activity in the decomposition of an industrial dye, a simulated effluent and levofloxacin under visible light irradiation with degradation efficiencies of 86%, 78% and 79%, respectively in 120 minutes compared to pure α-Bi_2O_3 (57%) under the same experimental conditions. The degradation of a

simulated dyebath effluent indicated that the composite has potential as a photocatalyst for treating wastewater on an industrial level. The enhanced photocatalytic efficiency of α-Bi_2O_3/C-dots is attributed to the C-dots which improved the light absorption capability of the nanocomposite and restricted the recombination of photogenerated electron−hole pairs. A mechanism for the degradation of the dye is proposed and explained on the basis of conformity to Langmuir Hinshelwood pseudo first order kinetics. In addition, α-Bi_2O_3/C-dots nanocomposite exhibited excellent recyclability and stability up to 3 cycles. This is considered beneficial for potential applications in environmental remediation. Radicals trapping studies concluded that electrons and hydroxyl radicals were the primary reactive species for the photocatalytic degradation of IC dye. The successful fabrication of a novel bismuth oxide based C-dots nanocomposite catalyst can be serve as a basis for fabricating other photocatalytic materials as catalysts for the degradation of other emerging pollutants of environmental concern.

Acknowledgements

Shelja Sharma would like to acknowledge UGC–BSR Government of India for providing financial support through a grant No. F. 25-1/2013(BSR)/5- 91/2007 (BSR) and Newton-Bhabha grant by DBT, Govt. of India and British Council, UK. The authors are grateful to TEQIP-III garnt of Dr. SSB University Institute of Chemical Engineering and Technology and SAIF, Panjab University, Chandigarh for providing the instrumental characterizations.

References

1. A.O. Ibhadon, P. Fitzpatrick, Heterogeneous photocatalysis: recent advances and applications, Catalysts 3 (2013) 189–218.
2. R. Lamba, A. Umar, S.K. Mehta, S.K. Kansal, ZnO doped SnO2 nanoparticles heterojunction photo-catalyst for environmental remediation, J. Alloys Compd. 653, (2015), pp. 327-333.

3. S. Kumar, S. Sharma, A. Umar, S.K. Kansal, Bismuth Sulfide (Bi_2S_3) nanotubes as an efficient photoctalyst for the methylene blue degradation, Nanosci. Nanotechnol. Lett. 8 (2016) 266–272.
4. A. Kaur, A. Umar, S.K. Kansal, Sunlight-driven photocatalytic degradation of non-steroidal anti-inflammatory drug based on TiO_2 quantum dots, J. Colloid Interface Sci. 459 (2015) 257–263.
5. S. Kaur, S. Sharma, S.K. Kansal, Synthesis of ZnS/CQDs nanocomposite and its application as a photocatalyst for the degradation of an anionic dye, ARS, Superlattices Microstruct. 98 (2016) 86–95
6. A. Kaur, A.O. Ibhadon, S.K. Kansal, Photocatalytic degradation of ketorolac tromethamine (KTC) using Ag-doped ZnO microplates, J Mater Sci. 52 (2017) 5256-5267.
7. L. Leonite, M. Caraman, M. Alexe, C. Harnagea, Structural and optical characteristics of bismuth oxide thin films, Surf. Sci. 507–510 (2002) 480–485.
8. H.F. Cheng, B.B. Huang, J.B. Lu, Z.Y. Wang, B. Xu, X.Y. Qin, X. Y. Zhang, Y.Dai, Synergistic effect of crystal and electronic structures on the visible-light-driven photocatalytic performances of Bi_2O_3 poly-morphs, Phys. Chem. Chem. Phys. 12 (2010) 15468–15475.
9. Q. J. Xiang, J. G. Yu, W. G. Wang and M. Jaroniec, Nitrogen self-doped nanosized TiO_2 sheets with exposed {001} facets for enhanced visible-light photocatalytic activity, Chem. Commun. 47 (2011) 6906-6908
10. W. Wang, J.C. Yu, Z. Shen, D.K.L. Chan, T. Gu, g-C_3N_4 quantum dots: direct synthesis, upconversion properties and photocatalytic application, Chem. Commun. 50 (2014) 10148-10150
11. Y. Hao, X. Dong, S. Zhai, X. Wang, H. Ma, X. Zhang, Controllable self-assembly of a novel Bi_2MoO_6-based hybrid photocatalyst: excellent photocatalytic activity under UV, visible and near-infrared irradiation, Chem. Commun. 52 (2016) 6525-6528.
12. S. Kumar, S. Sharma, S. Sood, A. Umar, S.K. Kansal, Bismuth Sulphide (Bi_2S_3) nanotubes decorated TiO2nanoparticles heterojunction assembly for enhanced solar light driven photocatalytic activity, Ceram. Int., 42 (2016) 17551–17557.

13. A. Kaur, S.K. Kansal, Bi_2WO_6 nanocuboids: An efficient visible light active photocatalyst for the degradation of levofloxacin drug in aqueous phase, Chem. Eng. J. 302 (2016) 194–203.
14. M.Q. Wen, T. Xiong, Z.G. Zang, W. Wei, X.T. Tang, F. Dong, Synthesis of MoS_2/g-C_3N_4 nanocomposites with enhanced visible-light photocatalytic activity for the removal of nitric oxide (NO), Opt. Express 24, (2016) 10205-10212.
15. S.N. Baker, G.A. Baker, Luminescent Carbon Nanodots: Emergent Nanolights, Angew Chem Int Ed. 49 (2010) 6726-6744.
16. H. Li, Z. Kang, Y. Liu, S.T. Lee, Carbon nanodots: synthesis, properties and applications, J. Mater. Chem. 22 (2012) 24230–24253.
17. B.Y. Yu, S.Y. Kwak, Carbon quantum dots embedded with mesoporous hematite nanospheres as efficient visible light–active photocatalysts, J. Mater. Chem. 22 (2012) 8345–8353
18. X. Wang, L. Cao, F.S. Lu, M.J. Meziani, H. Li, G. Qi, B. Zhou, B.A. Harruff, F. Kermarrec, Y.P. Sun, Photoinduced electron transfers with carbon dots, Chem. Commun. 25 (2009) 3774–3776
19. Y. Li, B.P. Zhang, J.X. Zhao, Z.H. Ge, X.K. Zhao, L. Zou, ZnO/carbon quantum dots heterostructure with enhanced photocatalytic properties, Appl. Surf. Sci. 279 (2013) 367–373
20. J. Wang, M. Gao, G.W. Ho, Bidentate-complex-derived TiO_2/carbon dot photocatalysts: in situ synthesis, versatile heterostructures, and enhanced H_2 evolution, J Mater Chem A 2 (2014) 5703- 5709.
21. H.C. Zhang, H. Ming, S. Lian, H. Huang, H. Li, L. Zhang, et al. Fe_2O_3/carbon quantum dots complex photocatalysts and their enhanced photocatalytic activity under visible light, Dalton trans. 40 (2011) 10822-10825.
22. H. Yu, H. Zhang, H. Huang, Y. Liu, H. Li, H. Ming, Z. Kang, ZnO/carbon quantum dots nanocomposites: one-step fabrication and superior photocatalytic ability for toxic gas degradation under visible light at room temperature, New J Chem. 36 (2012) 1031- 1035.

23. C.C. Chen, T. Fan, Study on carbon quantum dots/$BiFeO_3$ heterostructures and their enhanced photocatalytic activities under visible light irradiation, J. Mater. Sci.: Mater. Electron. 28 (2017) 10019-10027.
24. Y. Ye, Z. Zhang, T. Zhou, F. Dong, S. Lu, X. Tang, W. Wei, Y. Zhang, Theoretical and experimental investigation of highly photocatalytic performance of CuInZnS nanoporous structure for removing the NO gas, J. Catal. 357 (2018) 100-107.
25. S. Sharma, S.K. Mehta, S.K. Kansal, N doped ZnO/C-dots nanoflowers as visible light driven photocatalyst for the degradation of malachite green dye in aqueous phase, J. Alloys Compd. 699 (2017) 323-333.
26. J. Di, J. Xia, M. Ji, H. Li, H. Xu, H. Li, R. Chen, The synergistic role of carbon quantum dots for the improved photocatalytic performance of Bi_2MoO_6, Nanoscale 7 (2015) 11433-11443.
27. D. Tang, H. Zhang, H. Huang, R. Liu, Y. Han, Y. Liu, C. Tong, Z. Kang, Carbon quantum dots enhance the photocatalytic performance of $BiVO_4$ with different exposed facets, Dalton Trans. 42 (2013) 6285-6289.
28. Y. Chen, Q. Lu, X. Yan, Q. Mo, Y. Chen, B. Liu, L. Teng, W. Xiao, L. Ge, Q. Wang Enhanced Photocatalytic Activity of the Carbon Quantum Dot-Modified BiOI Microsphere, Nanoscale Res. Lett. 11 (2016) 60.
29. C. Zhao, W. Li, Y. Liang, Y. Tian, Q. Zhang, Synthesis of BiOBr/carbon quantum dots microspheres with enhanced photoactivity and photostability under visible light irradiation, Appl. Catal. A 527 (2016) 127–136.
30. J. Di, J. Xia, X. Chen, M. Ji, S. Yin, Q. Zhang, H. Li, Tunable oxygen activation induced by oxygen defects in nitrogen doped carbon quantum dots for sustainable boosting photocatalysis, Carbon 114 (2017) 601–607
31. X.Y. Kong, W.L. Tan, B.J. Ng, S.P. Chai, A.R. Mohamed, Harnessing Vis–NIR broad spectrum for photocatalytic CO_2 reduction over carbon quantum dots-decorated ultrathin Bi_2WO_6 nanosheets, Nano Res. 10 (2017) 1720–1731
32. X. Qian, D. Yue, Z. Tian, M. Reng, Y. Zhu, M. Kan, T. Zhang, Y. Zhao, Carbon quantum dots decorated Bi_2WO_6 nanocomposite with enhanced photocatalytic oxidation activity for VOCs, Appl. Catal., B 193 (2016) 16–21.

33. R. Xie, L. Zhang, H. Xu, Y. Zhong, X. Sui, Z. Mao, Construction of up-converting fluorescent carbon quantum dots/$Bi_{20}TiO_{32}$ composites with enhanced photocatalytic properties under visible light, Chem. Eng. J. 310 (2017) 79–90
34. X. Wu, J. Zhao, S. Guo, L. Wang, W. Shi, H. Huang, Y. Liu, Z. Kang, Carbon dot and $BiVO_4$ quantum dot composites for overall water splitting via a two-electron pathway, Nanoscale 8 (2016) 17314-17321.
35. J. Di, J. Xia, M. Ji, B. Wang, S. Yin, H. Xu, Z. Chen, H. Li, Carbon Quantum Dots Induced Ultrasmall BiOI Nanosheets with Assembled Hollow Structures for Broad Spectrum Photocatalytic Activity and Mechanism Insight, Langmuir 32 (2016) 2075−2084.
36. W. Lin, X. Yu, Y. Shen, H. Chen, Y. Zhu, Y. Zhang, H. Meng, Carbon dots/BiOCl films with enhanced visible light photocatalytic performance, J. Nanopart. Res. 19 (2017) 56.
37. Y. Sun, Z. Zhang, A. Xie, C. Xiao, S. Li, F.Huang, Y. Shen, An Ordered and Porous N-doped Carbon Dot-1 Sensitized Bi2O3 Inverse Opal with Enhanced Photoelectrochemical Performance and Photocatalytic Activity, Nanoscale 7 (2015) 13974-13980.
38. S. Sharma, A. Umar, S.K. Mehta, S.K. Kansal, Fluorescent spongy carbon nanoglobules derived from pineapple juice: A potential sensing probe for specific and selective detection of chromium (VI) ions, Ceram. Int. 43 (2017) 7011-7019.
39. S. Sood, A. Umar, S.K. Mehta, S.K. Kansal, α-Bi2O3 nanorods: An efficient sunlight active photocatalyst for degradation of Rhodamine B and 2,4,6-trichlorophenol, Ceram. Int. 41 (2015) 3355–3364
40. Z. Ai, Y.Huang, S.Lee, L.Zhang, Monoclinic-Bi_2O_3 photocatalyst for efficient removal of gaseous NO and HCHO under visible light irradiation, J. Alloys Compd. 509 (2011) 2044–2049.
41. S. Liu, J. Tian, L. Wang, Y. Zhang, X. Qin, Y. Luo, et al., Hydrothermal treatment of grass: a low-cost, green route to nitrogen-doped, carbon-rich, photoluminescent polymer nanodots as an effective fluorescent sensing platform for label-free detection of Cu(II) Ions, Adv. Mater. 24 (2012) 2037–2041.
42. H. J. Jung, S. Park, K. D. Kim, T. H. Kim, M. Y. Choi, K. Y. Lee, Fabrication of porous β-Bi_2O_3 nanoplates by phase transformation of bismuth precursor via low-temperature thermal decomposition process and their enhanced photocatalytic activity, Colloids Surf., A 550 (2018) 37–45.

43. A. Mewada, S. Pandey, S. Shinde, N. Mishra, G. Oza, M. Thakur, M. Sharon, M. Sharon, Green synthesis of biocompatible carbon dots using aqueous extract of Trapa bispinosa peel, Mater. Sci. Eng. C Mater. Biol. Appl. 33 (2013) 2914–2917.
44. Y. Xiong, M.Wu, J.Ye, Q.Chen, Synthesis and luminescence properties of hand-like α-Bi_2O_3 microcrystals, Mater. Lett. 62 (2008) 1165–1168.
45. W.T. Dong C.S. Zhu, Optical properties of surface-modified Bi_2O_3 nanoparticles, J. Phys. Chem. Solids 64 (2003) 265–271.
46. Q. Xiang, J. Yu and M. Jaroniec, Enhanced photocatalytic H_2 production activity of graphene-modified titania nanosheets, Nanoscale 3 (2011) 3670–3678.
47. N. Barka, A. Assabbane, A. Nounah, Y.A. Ichou, Photocatalytic degradation of indigo carmine in aqueous solution by TiO_2-coated non-woven fibres, J. Hazard. Mater. 152 (2008) 1054-1059.